Multilamellar Nanovectors composed of Microbial Glycolipid-Polylysine Complexes for Drug Encapsulation

Silvia Alonso-De-Castro, Sergio Oliveira Formoso, Chloé Seyrig, Korin Ozkaya, Julien Dumond, Luisa Riancho, Javier Perez, Christophe Hélary, Niki Baccile

Multilamellar Nanovectors composed of Microbial Glycolipid-Polylisine Complexes for Drug Encapsulation

Silvia Alonso-de-Castro[a], Sergio Oliveira Formoso[a], Chloé Seyrig[a], Korin Ozkaya[a], Julien Dumont[b], Luisa Riancho[c], Javier Perez[d], Christophe Hélary[a,*], Niki Baccile[a,*]

[a] Sorbonne Université, Centre National de la Recherche Scientifique, Laboratoire de Chimie de la Matière Condensée de Paris, LCMCP, 75005 Paris, France.
[b] Centre interdisciplinaire de recherche biologique, Collège de France, 75005 Paris, France.
[c] Centre de Recherche Institut de la Vision, UMR_S968 Inserm / UPMC / CHNO des Quinze-Vingts, 75012 Paris, France.
[d] Synchrotron Soleil, L'Orme des Merisiers, Saint-Aubin, BP48, 91192 Gif-sur-Yvette Cedex, France.

Abstract
This study addresses the potential use of single-glucose microbial amphiphiles as phospholipid-free drug carriers. Microbial amphiphiles, also known as biosurfactants, are molecules obtained from the fermentation of bacteria, fungi or yeast and largely studied for their antimicrobial, cleaning or anti-pollution potential. However, recent understanding of their self-assembly properties combined to their interactions with macromolecules suggest broader potential applications, one being the phospholipid-free conception of drugs. In this study, we want to demonstrate that this class of bio-based molecules can be directly used to design colloidally-stable vesicular carriers for hydrophobic drugs, without employing phospholipid supports, and that the actives can be delivered to human cells. In this study, multilamellar wall vesicles (MLWVs) have been synthesised using a microbial glycolipid amphiphile and polylysine, held together by electrostatic attractive interactions. Curcumin, a highly lipophilic molecule, was used as natural drug model to evaluate the present colloidal system as potential nanocarrier. The cell uptake of the curcumin-loaded nanocarriers was significantly higher for HeLa cells (50 %) compared to Normal Human Dermal Fibroblasts (35 %) and to THP-1 derived macrophages (20 %). The cytotoxic effect of delivered curcumin or other pharmaceuticals (Doxorubicin, Docetaxel, Paclitaxel) was higher in HeLa cells as the cell viability was reduced by 50 %.

Introduction
Biological amphiphiles, often referred to as biosurfactants, represent a class of amphiphilic molecules synthesised by microorganisms, garnering considerable attention for their heightened eco-sustainable profile [1]. Within the spectrum of the available biosurfactant families, glycolipids emerge as particularly relevant macromolecules. Their relevance stems from their high throughput production process and a wide range of applications, with a focus on their use in the biomedical domain, notably in antibiotic development [2].

The scientific community has so far dedicated some effort in exploring the anticancer properties of microbial glycolipids (e.g., sophorolipids) [3–5], with an ongoing debate about their effect [6]. Only little work has described the possibility to develop biosurfactant-based carriers [7] from these molecules. Actually, nanocarriers are predominantly composed of phospholipid liposomes [8,9]. Consequently, a more comprehensive work on the impact of biosurfactants on pre-formed bilayer membranes, their

structural intricacies, and the potential to deliver drugs is imperative for the assessment of high-quality lipid-based delivery systems [10–13].

In the recent years, the advances in the discovery, understanding and control of the self-assembly properties of microbial glycolipid amphiphiles has opened the opportunity to formulate phospholipid-free and stimuli-responsive complex colloidal structures exclusively composed of bioamphiphiles [14,15]. Multilamellar wall vesicles (MLWV), member of the polyelectrolyte-surfactant complexes family, are interesting colloidal assemblies with notable relevance in the biomedical field. For instance, MLWV have been previously employed in gene transfection studies, due to their increased stability compared to single-wall vesicles [16]. Our recent investigations revealed the feasibility of manipulating the attractive electrostatic interactions between the microbial C18:1-*cis* single glucose lipid (G-C18:1, GC, Figure 1), a type of microbial glycolipid with a stunning colloidal behaviour [17], and poly-L-lysine (PLL) at the micelle-to-vesicle phase transition of the GC. Through this approach, we demonstrated the formation of colloidally-stable, phospholipid-free, MLWVs featuring a lamellar architecture composed of alternating layers of GC and PLL. These MLWVs are prepared from a pH-stimulated phase transition in aqueous medium, occurring approximately at pH 7 [18,19]. Furthermore, GC presents an interesting asymmetric bolaform structure with a free-standing COOH group, which makes the molecules pH-sensitive with a more complex phase behaviour than classical lipids or surfactants [15].

Drug delivery systems are advanced technologies designed to facilitate targeting and/or controlled release of active pharmaceutical drugs. These systems address numerous challenges associated with the systemic administration of free pharmacological molecules, thereby enhancing their therapeutic efficacy. This improvement is achieved by mitigating several side effects, modulating solubility-related complexities, enhancing biological stability and optimising clearance while minimising non-specific delivery [20]. Drug delivery systems are often in the form of a drug carrier, serving the dual purpose of specific distribution and protection of the active pharmacological principle from degradation and removal by the reticuloendothelial system (RES) [21]. Several examples of such delivery systems have been extensively reported in the literature, highlighting the use of liposomes [22], synthetic polymers [23] or a combination of both [24], but also polymeric micelles [25], peptide-based biomaterials [26], inorganic nanoparticles [27]**,** gels [28] and biopolymer/clay hybrids [29]. Notably, liposomes, with their characteristic bilayer assembly resembling native extracellular membranes, ease of preparation, and biocompatibility, stand out as the most commonly investigated nanocarriers for drug encapsulation [22]. Despite their benefits, phospholipid liposomes face several drawbacks including triggering the immune response and RES clearance [30]. Therefore, there is a significant need for new alternatives to engineer novel drug delivery systems that can overcome these issues.

In this context, it is of particular interest to evaluate the performance of engineering MLWV composed of a (non-acetylated acidic) single-glucose microbial glycolipid and a biocompatible polyelectrolyte as a nanocarrier to deliver hydrophobic and hydrophilic drugs, to diminish their clearance and increase their bioavailability [31,32]. We present here a study on drug loading, cell delivery and cytotoxicity of MLWV composed of the microbial single-glucose lipid, GC, and the biocompatible polyelectrolyte, PLL, (GCPLL MLWV). This work has focused on the delivery of curcumin, a natural drug studied in a number of nanoscale carriers [33], and broadened to other commercial drugs, like doxorubicin, docetaxel and paclitaxel. Representative studies were performed in cells with different proliferative potentials:

mouse fibroblasts (L929), normal human dermal fibroblasts (NHDF), THP-1 derived macrophages and human cervical carcinoma cells (HeLa).

1. Materials and Methods

1.1. Materials

Microbial glycolipid G-C18:1 (M_W = 462 g.mol^{-1}), here shortened as GC for naming purposes, is composed of a non-acetylated acidic single *β*-D-glucose headgroup and a C18:1 fatty acid tail (monounsaturation in position 9 and 10). The GC glycolipid (lot nº APS F06/F07 Inv96/98/99) was purchased from Amphistar (Gent, Belgium), produced by the Bio Base Europe Pilot Plant (Gent, Belgium), and used without further modification. The molecule was obtained by fermentation from the yeast *Starmerella bambicola ΔugtB1*, according to a previously reported protocol [34]. From the specification sheet provided by the producer, the batch (99.4 % dry matter) was composed of 99.5 % GC according to HPLC-ELSD chromatography data. NMR analysis of the same compound (different batch) was performed elsewhere [14]. GC molecular purity was higher than 95 %. Poly-L-lysine hydrobromide (PLL, 1-5 KDa), Curcumin (*Cur*), lipopolysaccharides (LPS), phorbol 12-myristate 13-acetate (PMA), paraformaldehyde (PFA), docetaxel, paclitaxel, and doxorubicin were purchased from Sigma-Aldrich. Lissamine rhodamine B sulfonyl ammonium salt (18:1 Liss-Rhod PE, *Rhod*, M_w = 1301.7 g.mol^{-1}) was purchased from Avanti Polar Lipids. 4',6-diamidino-2-phenylindole dihydrochloride (DAPI) was purchased from Life Technologies. All chemicals were of reagent grade and were used without further purification unless otherwise specified.

1.2. Cell culture

L929 mouse fibroblasts, HeLa human cervical carcinoma cells and normal human dermal fibroblasts (NHDF) were purchased from Merck and cultured in Dulbecco's Modified Eagle Medium (DMEM, Sigma) supplemented with 10 % foetal bovine serum (FBS, Sigma), 1 % penicillin/streptomycin (PS, Sigma) and 1 % amphotericin B (Amph-B, Sigma). THP-1 human derived monocytes were purchased from Promocell and cultured in RPMI 1640 medium (Sigma) supplemented with 10 % FBS, 1 % PS and 1 % Amph-B. Cells were then cultured in an incubator at 37 °C and 5 % CO_2 under 100 % humidity.

1.3. Preparation of GCPLL MLWVs

GCPLL MLWVs were prepared according to previously published protocols [18,19] . In brief, stock solutions were prepared by dissolving 5 mg of GC or PLL in 1 mL of DMEM supplemented with 10 % FBS. Both solutions were raised to pH 10 with small volumes of 1 M NaOH, a step necessary to solubilise GC to a micellar phase, and mixed with PLL in a 1:1 volume ratio followed by vortexing. The final concentration of GC and PLL was 2.5 mg.mL^{-1}. The pH of the mixture was then lowered to 7 with small volumes of HCl 1 M to trigger the formation of MLWVs. At this point, the solution was slightly cloudy, confirming the presence of MLWVs.

1.4. Encapsulation of Curcumin (Cur) in GCPLL MLWVs (GCPLL-Cur MLWV)

A 13.5 mM *Cur* stock solution was prepared in absolute ethanol by thoroughly mixing. After the formation of GCPLL MLWVs in cell culture medium at pH 7, 10 µL of *Cur* solution was added to 1 mL of GCPLL MLWVs solution, reaching a final *Cur* concentration of 135 µM. After thoroughly vortexing, the suspension was centrifuged at 3000 RPM for 5 minutes to collect a pellet of GCPLL-*Cur* MLWVs. The

excess, non-encapsulated *Cur* present in the supernatant was removed, and the pellet resuspended in fresh cell culture medium by vortexing.

1.5. Encapsulation of doxorubicin, paclitaxel and docetaxel in GCPLL MLWVs

Stock solutions of anticancer drugs were prepared to by diluting doxorubicin in DMSO (1 $mg.mL^{-1}$), paclitaxel in ethanol (0.1 $mg.mL^{-1}$) and docetaxel in ethanol (0.1 $mg.mL^{-1}$). In a similar process to that described for the encapsulation of *Cur*, aliquots of 10 µL of each anticancer drug solution were added to 1 mL of GCPLL MLWVs solution, following the same protocol of centrifugation and resuspension in fresh cell culture medium.

1.6. Drug-loading characterisation

The loading capacity (LC %) was calculated as the ratio between the amount of encapsulated curcumin (*Cur*) over the total amount of delivery vehicles (GCPLL MLWVs), and expressed as a percentage (Eq. 1). The encapsulation efficiency (EE %) was calculated by dividing the amount of encapsulated *Cur* by the total amount of *Cur* used during the encapsulation process, and expressed as a percentage (Eq. 2).

$$Loading\ Capacity\ (LC\%) = \frac{mass\ of\ encapsulated\ Cur}{mass\ of\ GCPLL} \times 100 \qquad \text{Eq. 1}$$

$$Encapsulation\ Efficiency\ (EE\%) = \frac{mass\ of\ encapsulated\ Cur}{mass\ of\ loaded\ Cur} \times 100 \qquad \text{Eq. 2}$$

1.7. *Labelling of GCPLL MLWVs and GCPLL-Cur MLWVs with rhodamine (GCPLL-Rhod MLWVs and GCPLL-Cur-Rhod MLWVs)*

Both GCPLL MLWVs and GCPLL-*Cur* MLWVs solutions were prepared as previously described. For their labelling using *Rhod*, 10 µL of *Rhod* solution in ethanol (4 $mg.mL^{-1}$, 3.08 mM) was added to the corresponding solution so that the GC:*Rhod* molar ratio is 200:1. After vortexing, the solution was centrifuged at 3000 g for 5 minutes and the pellet resuspended in fresh cell culture medium. *Rhod* is a standard dye to label lipid bilayers, as its lipid backbone intercalates in this bilayer without any perturbation when the lipid-dye molar ratios is ≥ 100 [35,36].

1.8. *Small Angle X-Ray Scattering (SAXS)*

pH-resolved *in situ* SAXS experiments were performed at room temperature on the Swing beamline at Soleil Synchrotron (Saint-Aubin, France) under the proposal nº 20190961. The beam energy was E = 12 keV, the detector was Eiger X 4M, and the sample-to-detector distance was 1.995 m. Silver behenate [d(001) = 58.38 Å] was used as standard to calibrate the q-scale. Raw data collected on the 2D detector was integrated azimuthally using the in-house Foxtrot software provided at the beamline to obtain the typical scattered intensity I(q) profile, with q being the wavevector [$q = (4\pi \sin \Phi)/\lambda$; where 2Φ is the scattering angle and λ is the wavelength]. Defective pixels and beam stop shadow were systematically masked before azimuthal integration. Absolute intensity unites were calibrated by measuring the scattering signal of water ($I(H_2O) = 0.0163\ cm^{-1}$). SAXS profiles were processed with SasView software (v.3.1.2, sasview.org). The experimental setup was reproduced from previously published work [18]. Briefly, the sample solution (1 mL, [CG]=[PLL]=2.5 mg/mL in DMEM, pH 11) was maintained in an external beaker under stirring conditions at room temperature (23 ± 2 °C). The solution was continuously flashed through a 1 mm glass capillary using an external peristaltic pump. The pH of the solution in the beaker was changed using an interfaced push syringe, injecting microliter amounts of a

0.5 M HCl solution. pH was measured using a microelectrode (Mettler-Toledo) and its value was monitored live and manually recorded from the control room. Considering the fast pH change kinetics, the error on the pH value was established as ± 0.1.

1.9. Polarised light microscopy (PLM)

PLM images were obtained using a Zeiss AxioImager A2 POL optical microscope in transmission mode, equipped with a polarised light source, crossed polarisers, and an AxioCam CDD camera. Images were obtained from a drop of the given sample solution deposited on a glass slide covered with a cover slip.

1.10. ^{1}H solution nuclear magnetic resonance (NMR)

Experiments of the different samples were recorded on an AVANCE III Bruker 300 NMR spectrometer using standard pulse programs and a 5 mm ^{1}H-X BBFO probe. The number of transients was 32 with 7.3 s recycling delay, 2.73 s acquisition time, and a receiver gain of 322. Chemical shifts are reported in parts-per-million (δ, ppm) and referenced to 3-(trimethylsilyl)propionic-2,2,3,3-*d*4 acid sodium salt (TMSP-*d*4, Sigma) with a peak at 0 ppm at 1 mg.mL^{-1} (5.8 mM). Experiments were performed using a 5 mm NMR tube containing 500 µL solution obtained by solubilising the GCPLL MLWVs pellet in MeOD. The pellet was obtained by centrifugation at 3000 RPM for 5 minutes. Signals at δ(PLL) = 2.8 ppm (t) and δ(GC) = 2.25 ppm (t) were used for calculations. All samples were prepared using this protocol and all experiments were performed under the same conditions unless otherwise specified. Results and figures are shown in the supplementary information (pages S2-S5).

1.11. UV-visible spectrometry

UV-visible absorbance spectra of curcumin solutions were collected using a Uvicon Spectrometer. Spectra were recorded by measuring absorbance of Curcumin at wavelengths in the range of 190-700 nm.

1.12. Cell viability assay

Cell viability experiments were performed with L929 to determine the optimal GCPLL MLWVs concentration. Cells were seeded on 24-well plates at a density of 5x10^{4} cells.mL^{-1} and cultivated for 24 hours. The following day, GCPLL MLWVs solutions with concentrations up to 122 µg.mL^{-1} were added and cells were cultivated for another 24-hour period. Furthermore, L929 cultures were exposed to free GC, PLL and DMEM with pH variations. Control samples were cultured in complete medium (supplemented with 10 % foetal bovine serum). Cell viability was determined by measuring their metabolic activity using the Alamar Blue Cytotoxicity Assay. Briefly, GCPLL MLWVs were removed from the culture wells and cells were rinsed twice with fresh medium. Then, 300 µL of 0.01 % w/v resazurin solution in fresh red phenol-free DMEM medium was added to cells and incubated for 4 hours. The supernatant from each well was then collected, further diluted with 700 µL of fresh red phenol-free medium, and 100 µL transferred to a 96-well plate to measure absorbance values at λ = 570 nm and λ = 600 nm. The percentage of resazurin reduction was calculated according to supplier instructions and compare to control samples. Then, the effect of GCPLL MLWVs, GCPLL-*Cur* MLWVs and *Cur* on the viability was assessed on three different human cell lines (HeLa, NHDF, THP-1). HeLa and NHDF were seeded on 24-well plates at a density of 5x10^{4} cells.mL^{-1} for 24 hours prior to the beginning of the experiment. Non-adherent THP-1 cells were seeded at a density of 5x10^{4} cells.mL^{-1} in 24-well plates and cultured for 24 hours with serum free RPMI 1640 medium supplemented with 100 ng.mL^{-1} PMA

to differentiate them into adherent macrophage-like cells. Then, differentiation medium was replaced by fresh complete RPMI 1640 medium for another 24-hour period. At this point, different concentrations of GCPLL MLWVs were added to the three different cell lines, and following a 24-hour culture time, the same Alamar Blue protocol previously described was performed for cell viability evaluation. Finally, cell metabolic activity between samples was compared. The arbitrary value of 100 % was given to controls. All experiments were carried out using at least three replicates and the results expressed as mean values ± standard deviation (SD). Statistical significance was analysed by XLSTAT using the Kruskal-Wallis test with $p<0.05$ considered as significant.

1.13. Optical fluorescence microscopy

Cells were seeded in 6-well plates at a density of $5x10^4$ cells.mL^{-1} and grown for a period of 24 hours under the conditions previously specified. Following, solutions of GCPLL MLWVs, GCPLL-*Cur* MLWVs, GCPLL-*Rhod* MLWVs, and GCPLL-*Cur*-*Rhod* MLWVs were added to cultured cells at a final concentration of 100 µg.mL^{-1} and incubated for another 24-hour period. Then, after three rinses with PBS, samples were fixed for 1 hour using 4 % PFA solution. Following another rinse step with PBS, cells were permeabilised for 15 minutes using a 0.2 % (v/v) PBS-Tween solution. Then, 300 µL/well of 1:50000 DAPI solution were added and cells incubated for 10 minutes. Finally, after another rinse step, cells were kept at 4 °C, protected from light, until further experimentation. Tagged cells were observed using a ZEISS fluorescence microscope equipped with an AxioCam MRm.

1.14. Flow cytometry analysis

Cells were seeded in 6-well plates at a density of $1x10^5$ cells/well, initially cultured for 24 hours. Then, cells were treated with a MLWVs solution of 100 µg.mL^{-1} and further incubated during another 24-hour period. Cultured cells were detached using trypsin, collected, and centrifuged at 900 g for 5 minutes. The cell pellet was resuspended in 1 mL 0.5 % PFA solution prepared in PBS. Flow cytometry was performed on a CELESTA SORP flow cytometer (BD Biosciences, USA). Acquisition gate was set to record 105 event total for each sample.

1.15. Confocal laser scanning microscopy

Samples were prepared using the same protocol explained for optical fluorescence microscopy, except that cell were cultured in a Thermo Scientific™ Nunc™ Lab-Tek™ II Chamber Slide, with 2 wells for optimal visualisation. Analysis was performed in a spinning disk head X1 (Yokogawa) mounted on a Nikon Eclipse Ti inverted microscope. Cells were observed with a 60x/1.4 Plan Apo objective and a Hamamatsu Orca Flash SCMOS camera.

2. Results and discussion

2.1. GCPLL MLWVs are stable in cell culture medium

Multilamellar wall vesicles only composed of the glycolipid biosurfactant GC (Figure 1) and the polyelectrolyte PLL, named GCPLL MLWVs, has been previously reported to self-assembly in mQ-grade water below pH 7.5 [18,19]. *In situ* SAXS showed the appearance of two diffraction peaks, corresponding to a lamellar assembly, with period variations in the pH range between 8 and 5. These results were further confirmed by cryo-TEM and PLM, observing the vesicular shape, the multilamellar structure, and spherulites with a maltese cross under cross-polarisers. This work complements previous publications and focuses on the characteristics of these self-assembled multilamellar vesicular objects

in cell culture medium, fundamental to develop carriers for biological applications. Thus, a similar approach is presented in this work using PLM techniques.

A typical cell culture medium contains a wide variety of compounds such as salts, glucose, and amino acids; and it is also generally supplemented with proteins coming from foetal bovine serum (FBS). This biochemical complexity may alter the charge, composition and pH-range of stability of GCPLL MLWVs. In a process, similar to that described elsewhere [18,19], the GCPLL MLWVs were prepared by pH modulation in DMEM cell culture medium instead of water. Therefore, the potential interactions with the different biochemical compounds are of great interest. pH-resolved in situ synchrotron SAXS was performed on the GCPLL system varying the pH from alkaline to acidic conditions in DMEM, and the corresponding contour plot between q=0.1 and 0.4 $Å^{-1}$ is shown in Figure 1a. At about pH 5, two sharp diffraction peaks appeared, corresponding to the first q(001)= 0.171 $Å^{-1}$ and second q(002)= 0.341 $Å^{-1}$ order reflections of the MLWVs phase. These peaks evolved during pH decrease and this behaviour is exactly the same as the one previously observed in water [18,19]. Below approximately pH 5, a structural gap appeared at q(001), similar to that previously reported in water systems [18], revealing the transition between MLWV and PLL-free lamellar phase composed of GC only and characterised by a peak at q= 0.169 $Å^{-1}$. Therefore, SAXS experiments using synchrotron radiation, performed during the pH-controlled synthesis process, provide the necessary real-time structural information proving the existence of the multilamellar structure of the nanocarriers.

GCPLL MLWVs are birefringent under polarised light [19]. PLM was used to discriminate the shape of the self-assembled entities and to confirm the multilamellar structure in supplemented cell culture media. PLM images were obtained under white (Figure 1b1) and polarised light (Figure 1b2, b3) with polarisers at 0°-90° and 45°-135°, respectively. Additionally, PLM revealed the presence of spherulite structures displaying optical birefringence in the shape of typical maltese cross colocalised with the spheroids. These results are in agreement with previously published work[19] and confirm that the interactions between the different biochemical compounds present in the cell culture media do not affect the shape and self-assembly structure of GCPLL colloids in solution.

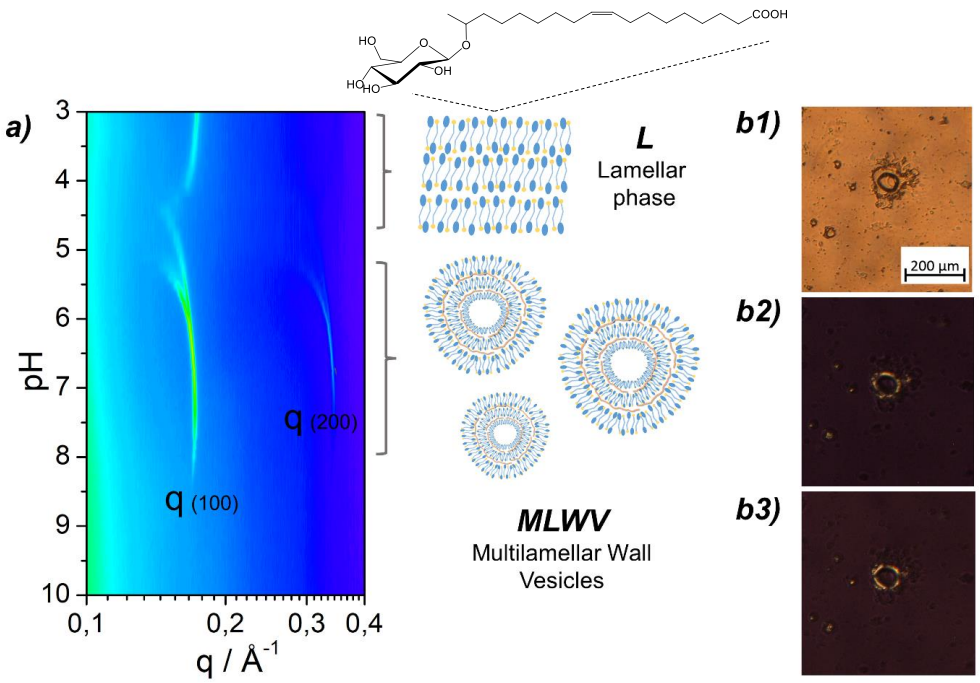

Figure 1. a) pH-resolved in situ SAXS (contour plot representation) experiments performed on 2.5 mg.mL^{-1} GCPLL (GC:PLL= 1:1) in DMEM cell culture medium. The schematic representation of the typical lamellar phase (L) and multilamellar wall vesicle assembly (MLWV) is also provided, with the chemical structure of the GC glucolipid. b1) PLM image of GCPLL MLWVs in DMEM culture medium containing birefringent patterns on the surface evidenced by the rotation of the polarisers from 45°-135° (b2) to 0°-90° (b3).

Previous work has shown that GCPLL MLWVs (2.5 mg.mL^{-1}, GC:PLL= 1:1) synthesised in water has a broad size distribution centered to about 700 nm [19]**.** It was demonstrated that classical methods to control their size, like filtration or tip-sonication, work well if needed. However, size control was out of the scope of the present manuscript. GCPLL MLWVs were stable for a pH ranging from 4 to approximately 7.5. The exact extreme pH value was not well defined and possible variations depend on experimental conditions, such as GC-to-PLL ratio or salt content [18,19]. The present work shows that the use of DMEM cell culture medium did not influence the formation of GCPLL MLWVs. Furthermore, it shows that the domain of pH stability was increased to higher values (approx. pH 8) compared to that found for pure water (Figure 1a). However, variations in the limits of the pH transition were not unexpected. GCPLL MLWVs are stabilised by attractive electrostatic forces between the negatively-charged GC and the positively-charged PLL. As previously demonstrated by NMR and isothermal titration calorimetry (ITC) [18], the negative and positive charges of these compounds vary with pH and ionic strength. In pure water and in the absence of supplementary salts, the optimal balance of charges for the MLWV phase starts at pH ~7.5. For DMEM cell culture medium, which is rich in salts, it was hypothesised that the optimal charge balance might occur at higher pH values, when part of the negative charges are counterbalanced by the free cations in solution.

Quantitative ^{1}H solution NMR, using methanol-*d*4 as the solvent, was employed to determine the content of GC and PLL within the MLWVs compared to the reference standard TMSP-*d*4. ^{1}H NMR spectra (Figures S1-S4) showed that GCPLL MLWVs in H_2O (pH=5.5) had a molar ratio of molecules consisting of 6.5 % of the initial content of PLL and 70 % of the initial content of GC. However, when GCPLL MLWVs were prepared in DMEM culture medium (pH=7.4), there was a proportional decrease

of both PLL and GC molar ratios, corresponding to 4 % and 45 % respectively (Table 1). A reduced content of both GC and PLL in samples prepared in DMEM compared to those prepared in water is in agreement with the higher pH values at which MLWVs were formed. As measured by SAXS (Figure 1a), GCPLL MLWVs were formed in the pH range of 4.5-8. Furthermore, the final molar ratio GC_f/PLL_f in H_2O and DMEM after the preparation of GCPLL MLWVs remained practically constant, at 57 and 60 respectively. The ratio between COOH and NH_2 functional groups, which partially reflects the charge ratio, was 2.8 and 3 for H_2O and DMEM respectively. Therefore, both the structural analysis and the composition of the GCPLL MLWVs support their stability at physiological pH in culture medium, and their further biological applications.

Table 1. Quantitative evaluation of GC and PLL in GCPLL MLWVs by ^{1}H solution NMR (further explanations on calculations described in Table S1). Subscripts: in= initial, f= final.

	C_{in} (mM)		C_f (mM)		C_f/C_{in} (%)		Molar ratio		Functional group
	$[GC]_{in}$	$[PLL]_{in}$	$[GC]_f$	$[PLL]_f$	$GC_{f/in}$	$PLL_{f/in}$	GC_{in}/PLL_{in}	GC_f/PLL_f	$[COOH]/[NH_2]$
H_2O	5.4	1	3.7	0.065	70	6.5	5.4	57	2.8
DMEM	5.4	1	2.4	0.04	45	4	5.4	60	3

2.2. GCPLL MLWVs are cytocompatible

To the best of our knowledge, the cytocompatibility of GCPLL MLWVs has not been reported. We evaluated their cytocompatibility on the L929 mouse fibroblast cell line diluting an initial 2.5 $mg.mL^{-1}$ mixture to obtain different concentrations from 0 to 1 $mg.mL^{-1}$. This concentration range was selected to be comparable with other examples on drug delivery systems, such as blank and loaded liposomes [37–39]. All the concentrations referred to the initial quantity employed in the preparation. Besides, the viability of cells was evaluated after incubation with GC and PLL independently. Furthermore, L929 viability was also evaluated with GC-free and PLL-free medium which has undergone the same pH changes required to prepare the GCPLL MLWVs. As shown in Figure 2a, there was no significant cytotoxicity effect for GCPLL MLWVs concentration at 50 $\mu g.mL^{-1}$. However, a detrimental effect on L929 metabolic activity was observed for concentrations at 122 $\mu g.mL^{-1}$ and 245 $\mu g.mL^{-1}$, with a 40 % and 80 % reduction respectively. Neither PLL treatment nor pH-dependent medium showed a significant cytotoxic effect under the studied conditions. However, GC treatment had a significant impact on L929 viability. For instance, a GC concentration of 250 $\mu g.mL^{-1}$ resulted in an approximately 20 % reduction in cell metabolic activity and a severe decrease of approximately 90 % is observed for GC concentrations higher than 500 $\mu g.mL^{-1}$.

According to ^{1}H solution NMR analysis (Figure S1-4 and Table S1), approximately 95 % of free PLL and 50 % of free GC were detected in a GCPLL colloidal solution in DMEM cell culture medium. For this reason, we hypothesised that most of the cytotoxic effect of the GCPLL MLWVs solution might be associated to free GC molecules. In order to prove this hypothesis, GCPLL MLWVs were prepared as usual but followed by a centrifugation step at 3000 g for 5 minutes. The supernatant was discarded to eliminate the free forms of GC and PLL, and fresh DMEM culture medium was added. In order to ensure that the colloidal stability was maintained and aggregation diminished, we vortexed and sonicated the solution for a few seconds. Zeta-potential measurements of GCPLL MLWVs in cell culture medium,

with a value of -11.9 ± 0.4 mV, confirmed a slight negative surface charge with positive outcomes in preventing aggregation [19,40,41]. Finally, as shown in Figure 2b, L929 viability after incubation with centrifuged GCPLL MLWVs showed no significant cytotoxicity up to 122 µg.mL^{-1} compared to the 50 % decreased shown when free GC was not removed.

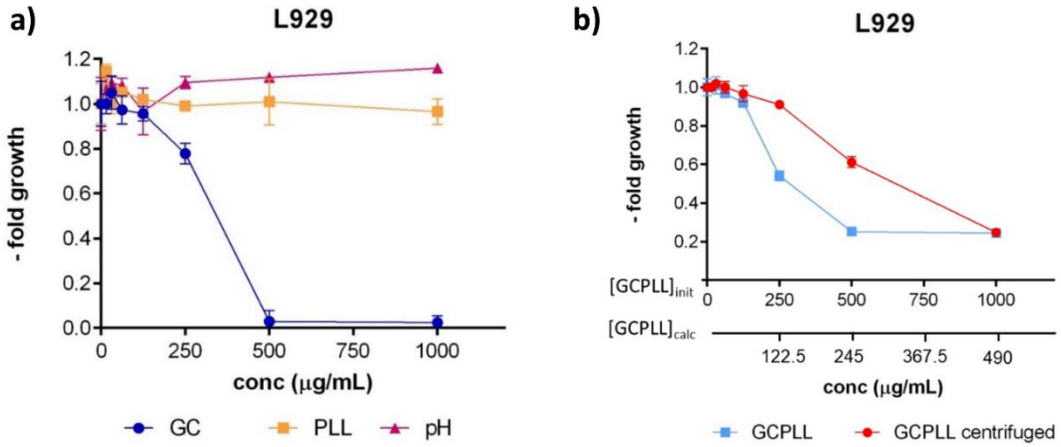

Figure 2. a) Cytocompatibility of GCPLL MLWVs, GC, PLL, and the effect of pH change on mouse fibroblast L929 cell line. In the pH change experiment, neither GC nor PLL are used and the pH is set at 7, after acidification from pH 10. b) Effect of removal of free GC on the cytocompatibility of GCPLL MLWVs. $[GCPLL]_{calc}$ refers to the concentration of GCPLL MLWVs after centrifugation, calculated by ^{1}H solution NMR as described in Table 1.

2.3. Curcumin is efficiently encapsulated within GCPLL MLWVs

The multilamellar lipid structure of GCPLL MLWVs, their stability in physiological culture medium and the absence of cytotoxicity make these self-assembled bodies interesting candidates as phospholipid-free drug delivery systems.

Curcumin (*Cur*), the active component of *Curcuma longa* plant, is a molecule widely used as a drug due to its antioxidant, anti-inflammatory and anticancer properties [42,43]. It is highly lipophilic, with a water-octanol partition coefficient (logP) in the order of 2.6 and a membrane partition constant above 10^4 M^{-1} [44]. Similar to other hydrophobic drugs [45], *Cur* has limited applicability due to its poor oral bioavailability, low chemical stability [46] and weak cellular uptake [42]. As a consequence, the accumulation of *Cur* is low within the cytoplasm as it interacts with the lipids of the cell membrane through H-bonding and hydrophobic interactions [47,48]. Different strategies were proposed in order to overcome these limitations such as the synthesis and use of curcumin derivatives [42], or the development of drug delivery systems which enhance its stability and increase its cellular uptake [49]. For this reason, we chose *Cur* as a model drug to load into the GCPLL MLWV system, with the aim of proving the encapsulation capability of the vesicles and to show their potential to enhance the therapeutic index of the encapsulated drug.

The zeta-potential measured on GCPLL-*Cur* MLWVs, the loaded vesicles exhibited a value of -13.2 ± 0.3 mV. The latter was not significantly different of the values mesured for unloaded systems (-11.9 ± 0.4 mV). These results are in line with the preservation of the colloidal stability after resuspension. UV-Visible absorbance measurements were performed to quantify the *Cur* encapsulated in GCPLL MLWVs just after preparation and after 24 hours of incubation in culture medium. As shown in Figure 3a, the absorption spectra were superimposable, thereby confirming that *Cur* was stable within the GCPLL

MLWVs solution over 24 hours and that it was encapsulated in its native form for concentrations up to 80 µM (Figure S5). Considering that previous reports have shown that free *Cur* decomposes by approximately 50 % in serum supplemented cell culture media after 8 hours incubation, we consider these results as a critical advantage.

Rhod is a well-known fluorescence phospholipid label which intercalates in the glucolipid membrane without interfering with the structure when the lipid-to-dye molar ratio is above 200 [50]. To confirm that *Cur* is actually colocalised in the GCPLL MLWVs and to exclude coprecipitation, we performed fluorescence microscopy imaging on a drop of GCPLL-*Cur* MLWVs solution that was simultaneously labelled with *Rhod*. As seen in Figure 3b, the colocalised fluorescence, red for *Rhod* and green for *Cur*, and the differential interference contrast microscopy (DIC) white light for GCPLL MLWVs confirmed the encapsulation of *Cur* within the GCPLL MLWVs.

A key parameter for the characterisation of drug delivery systems is the encapsulation efficiency (EE%), defined in Eq. 2. EE% varies according to different properties related to each system such as morphology, hydrophobicity, surface charge, permeability, the structure of the encapsulated molecule, and the encapsulation process itself [51,52]. Considering the molar concentration of *Cur* to be 80 µM, obtained by UV-VIS spectroscopy, and the total loaded *Cur* to be 135 µM; then EE% accounted to 60 %. This value was higher compared to other EE% values estimated for several vesicular systems, which shows a high variability ranging from 1 to 68 % for unilamellar vesicles (ULVs) and from 6 to 31 % for multilamellar vesicles (MLVs) [53]. The broad spectrum of reported EE% values between ULVs and MLVs is commonly explained by the presence of a lumen in ULVs, allowing to accommodate a higher loading volume of drug compared to the actual lipid content [53]. Despite the structural differences, we obtained EE% values comparable for both MLVs and ULVs. Another important parameter is the loading capacity (LC%), defined in Eq. 1. LC% is defined as the ratio between the amount of encapsulated *Cur*, which was 30 µg, and the weight of GCPLL MLWVs calculated by ^{1}H solution NMR, which was 1225 µg. We obtained a LC% value for the GCPLL-*Cur* MLWV system of approximately 2.5 %. Here, we hypothesise that the two-step preparation protocol for GCPLL-*Cur* MLWVs might explain the low values obtained for LC%. Considering that GCPLL MLWVs were already formed when *Cur* was added, encapsulation might occur only in the outer layers of the system. The strong discrepancy between LC% and EE% values might confirm this, leading to an optimal encapsulation process but a low drug-to-lipid content. While other protocols might improve both the EE% and LC% of this system, their study is out of the scope of the present work.

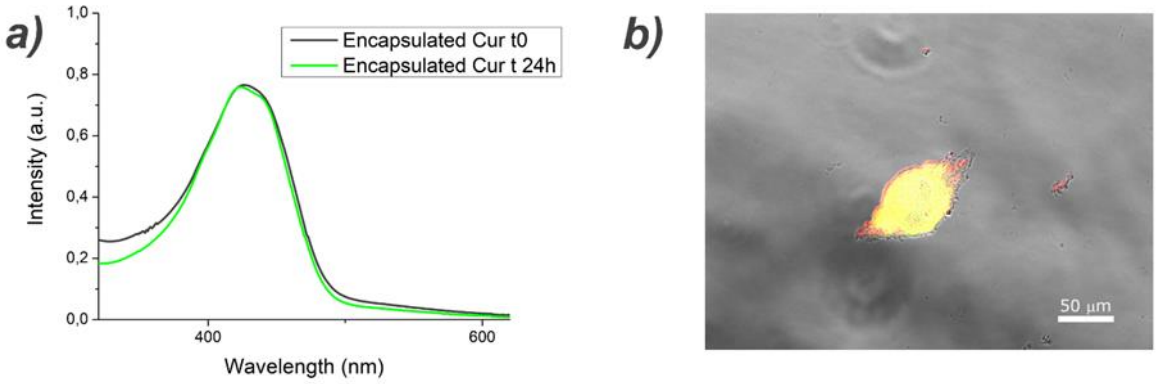

Figure 3. a) UV-Visible spectra of curcumin (*Cur*) encapsulated in GCPLL MLWVs at t=0 and t=24h in DMEM cell culture medium. GCPLL-*Cur* MLWVs were centrifuged and resuspended in ethanol for analysis. b) Fluorescence microscopy image of GCPLL-*Cur-Rhod* MLWVs at 2.5 mg.mL^{-1} in DMEM cell culture medium. *Rhod* (red) and *Cur* (green) were loaded within the particles.

2.4. GCPLL MLWVs can be used to deliver curcumin to human cells

The biological activity of GCPLL-*Cur* MLWVs was explored using three different human cell lines, as shown in Figure 4a-c. HeLa cells were chosen as a cancerous model with high proliferation, NHDF cells were chosen as a model with moderate proliferation and THP-1 derived macrophages used as not dividing cells. Also, macrophages are members of the RES characterised by their high phagocytic activity, which help to clear particles from the human body. Hence, the MLWVs uptake by macrophages could be related to the persistence of particles in blood.

The cytotoxic effect of free *Cur* was explored on each kind of cells as a control experiment. As shown in Figure 4d, the toxicity of free *Cur* was negligible for both THP-1 derived macrophages and NHDFs. However, there was a slight statistically relevant reduction on the viability of HeLa cells when the concentration of *Cur* was 5 µg.mL^{-1}, which decreased down to 75 % of metabolic activity measured for control samples. The cytotoxic effect of GCPLL MLWVs was negligible for both NHDF and THP-1 derived macrophages, as seen in Figure 4b,c. Therefore, only a slight decrease in cell viability was observed for HeLa cells at the highest concentration tested. As shown in Figure 4a, for a concentration of 122 µg.mL^{-1} of GCPLL MLWVs, HeLa cell viability remained higher than 80 % and therefore, no significant toxicity was observed.

GCPLL-*Cur* MLWV showed a different behaviour. Figure 4c showed that for loaded vesicles up to 122 µg.mL^{-1} there was no significant effect on THP-1 derived macrophages viability. Additionally, NHDF metabolic activity decreased down to 75 % when the concentration of GCPLL-*Cur* MLWVs reached 122 µg.mL^{-1}. In contrast, the effect of GCPLL MLWs on cancerous HeLa cells was dramatically different. Figure 4a showed a drastic decrease to about 50 % in cell viability for a concentration at 122 µg.mL^{-1}. Moreover, the cytotoxic effect of GCPLL-*Cur* MLWV was higher than the one of free *Cur* despite a lower amount of carrier. For a calculated 3 µg.mL^{-1} *Cur* content in the most toxic GCPLL-*Cur* MLWV sample, there was approximately 50 % cell viability; while for 5 µg.mL^{-1} free *Cur* concentration, cell viability was approximately 75 %. As the cytotoxic effect of *Cur* encapsulated within GCPLL MLWVs was greater for HeLa cells compared to NHDF and THP-1 derived macrophages, we hypothesise that the cytotoxic of *Cur* might be correlated with cell doubling time.

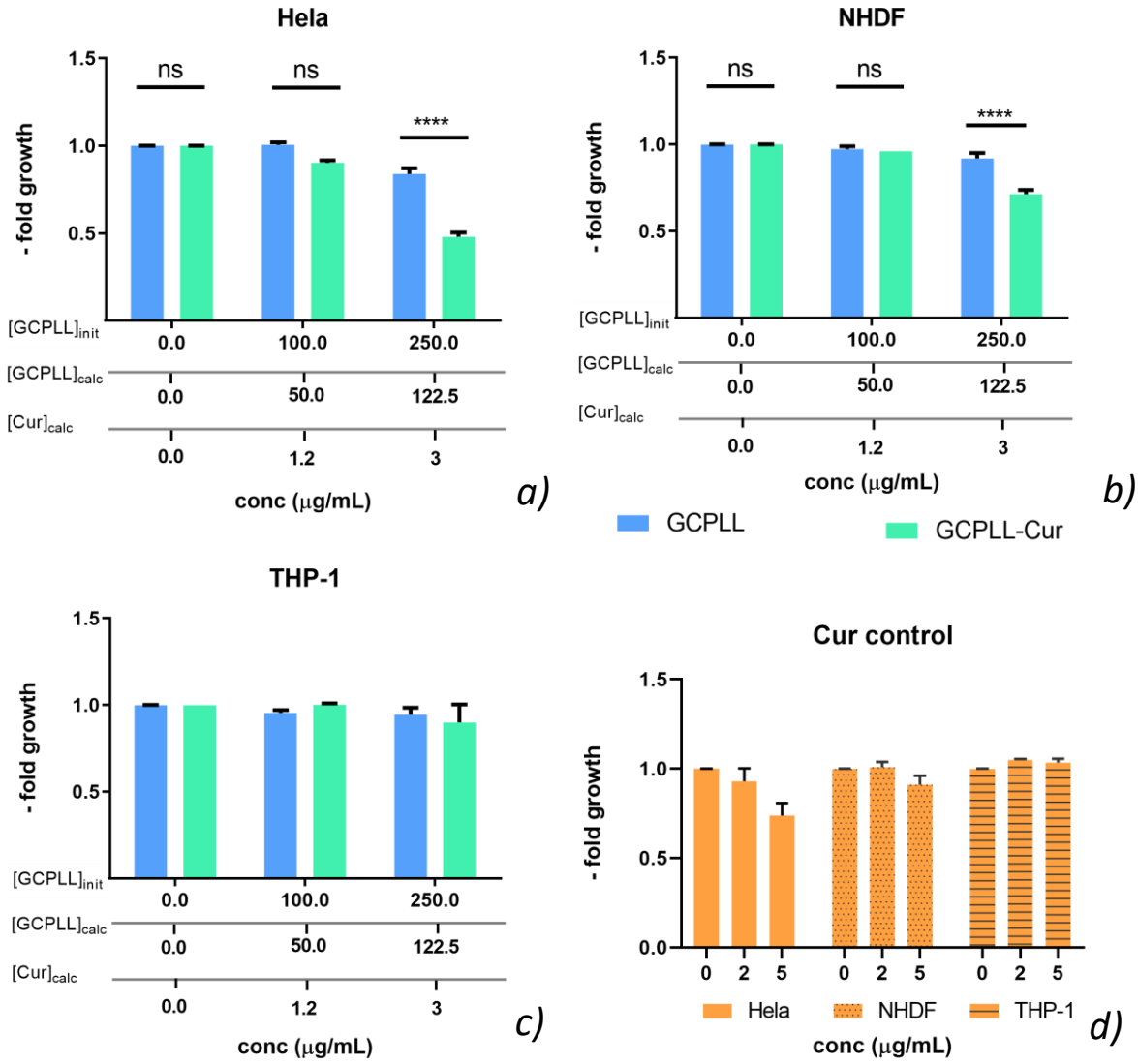

Figure 4. a-c) Cell viability of GCPLL MLWVs (blue), GCPLL-*Cur* MLWVs (green) in a) HeLa cells; b) NHDF cells; and c) THP-1 derived macrophages. Three abscissas are displayed to show the initial concentration employed in the preparation of the vesicles, the calculated GCPLL content and the *Cur* encapsulated. In particular, $[GCPLL]_{init}$ refers to initial concentration employed in the preparation of GCPLL MLWVs, $[GCPLL]_{calc}$ refers to concentrations calculated by ^{1}H solution NMR (Table 1) after centrifugation and resuspension of the GCPLL MLWV pellet, and $[Cur]_{calc}$ refers to the encapsulated *Cur* in the GCPLL MLWVs measured by UV-Vis (Figure 3). d) Cell viability of free *Cur* control in the three different cell types tested. Results are presented as mean ± SEM (n=3, *:p<0.05, Kruskal-Wallis test).

Other studies reported an half-maximal inhibitory concentration (IC_{50}) of 6.6 μM for carboxymethyl dextran (CMD)-modified liposomal *Cur* systems and an IC_{50} of 21 μM and 16 μM for *Cur*-loaded cationic liposomes using HeLa and SiHa cells, respectively, and can be comparable to ours [54,55]. These results evidence the remarkable activity of the GCPLL-*Cur* MLWV system towards cancerous HeLa cells. Moreover, with negligible cytotoxic effects on NHDF and non-dividing THP-1 derived macrophages, we hypothesise that this system might potentially avoid damage to normal tissues and the foreign particle elimination pathway through RES clearance.

Lipid-based particles can be uptaken by cells following different cellular mechanisms, i.e. nanoparticles ranging from 50 to 100 nm can be engulfed by endocytosis, those less than 400 nm by micropinocytosis, and micrometric particles can enter the cells by phagocytosis [56,57]. Considering that

the present GCPLL MLWVs population is polydisperse, of diameter ranging from 50 nm to 10 µm,[14] we hypothesise that internalisation might not be the most appropriate route for drug delivery. For example, macrophages are prone to engulf particles ranging from 1 to 5 µm by phagocytosis but particles were not observed within THP1 cells. In addition, cytotoxicity of curcumin encapsulated within GCPLL MLWVs seems to be correlated to the proliferative rate of cells.

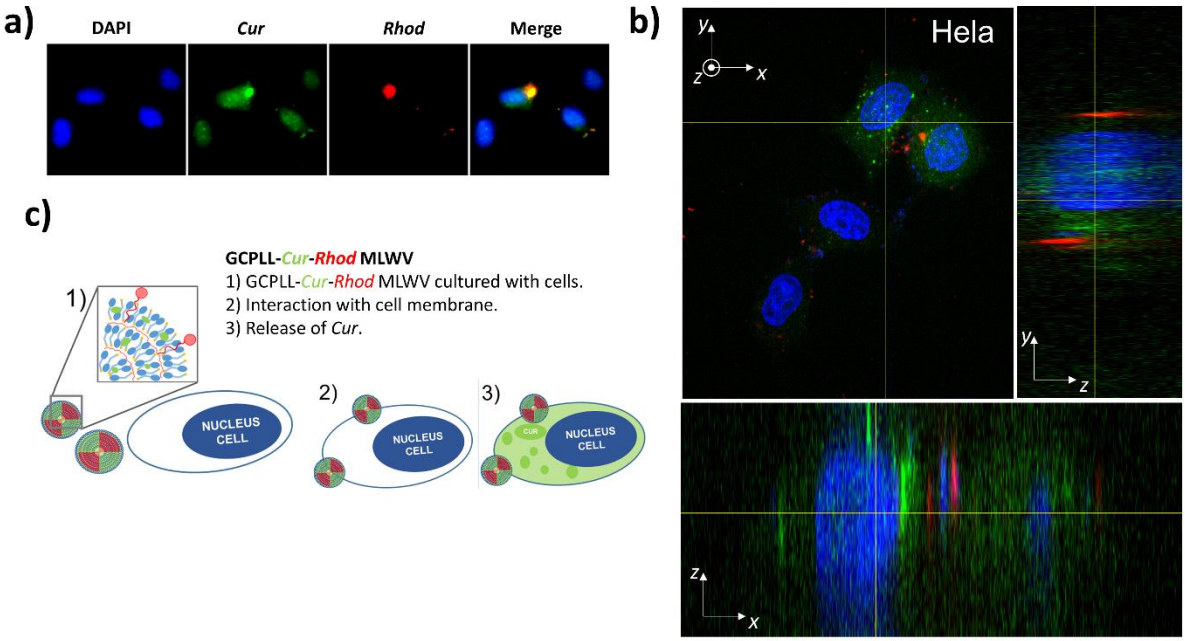

Figure 5. a) Fluorescence confocal microscopy images on HeLa cells treated with 100 µg.mL^{-1} of GCPLL-*Cur*-*Rhod* MLWVs. b) Orthogonal views obtained by confocal microscopy of HeLa cells treated with 100 µg.mL^{-1} GCPLL-*Cur*-*Rhod* MLWVs. Blue channel corresponds to the cell nucleus stained with DAPI, green channel corresponds to *Cur*, red channel corresponds to GCPLL MLWVs stained with *Rhod.* c) Schematic representation of the cellular uptake mechanism of GCPLL-*Cur*-*Rhod* MLWVs.

We designed here proof-of-concept experiments to explore the release mechanism of *Cur* to the HeLa cell cytoplasm using GCPLL-*Cur* MLWVs and better understand their cytotoxicity. As shown in Figure 5a, *Cur* is confined within the cell cytoplasm as observed by the green fluorescence signal surrounding the cell nucleus. The presence of *Cur* within the cytoplasm of HeLa cells can be further observed in Figure S6-7, which put in evidence the presence of green fluorescence grains only when HeLa cells were treated with GCPLL-*Cur* MLWVs. Moreover, the colocalization of *Cur* and *Rhod* in areas close to the cell membrane was evident, as observed in the yellow area on the merge image in Figure 5a. However, in order to further understand if vesicles were either internalised or retained within the cell membrane of HeLa cells, we performed confocal microscopy imaging. As shown in Figure 5b, HeLa cells treated with GCPLL-*Cur*-*Rhod* MLWVs clearly showed that GCPLL MLWVs, labelled in red with *Rhod*, were localised in the outer part of the cell membrane; while green areas corresponding to *Cur* are confined to the cytoplasm, surrounding the cell nucleus. A schematic representation of the uptake mechanism is illustrated in Figure 5c. As no red fluorescence signal was detected inside the HeLa cells, we understand that the delivery mechanism might not be governed by internalisation. Instead, we propose that GCPLL MLVWs might fuse or intertangle with the cell membrane to deliver *Cur* to the cell cytoplasm. However, further experimentation should be performed to corroborate these hypotheses.

Additionally, we also studied the interaction of the GCPLL MLWVs with NHDF and non-dividing THP-1 cells. As shown in figure 6a, green fluorescence grains are only observed within HeLa cells when the lamellar system is loaded with *Cur*. Flow cytometry measurements on the three cell lines tested, shown in figure 6b, evidence differences in the uptake of GCPLL MLWVs. Dividing cells (HeLa cells and NHDF) showed the highest percentage of *Rhod* label (around 40 % using GCPLL-Cur *Rhod* MLWVs, compared to THP-1 (15 % using GCPLL-Cur *Rhod* MLWVs). However, the detection of large quantities of curcumin within cells was only observed for Hela cells.

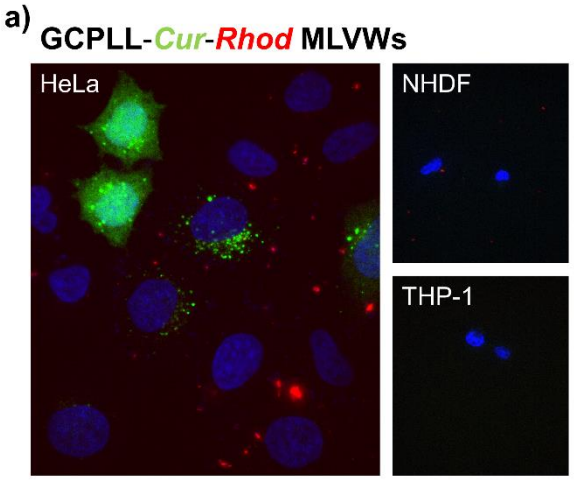

b)

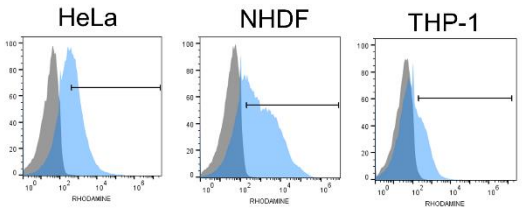

Flow cytometry	HeLa	NHDF	THP-1
GCPLL-*Rhod*	26.4 ± 0.6 %	46.8 ± 2.0 %	15.3 ± 10 %
GCPLL-*Cur-Rhod*	41.8 ± 9.2 %	33.3 ± 3.0 %	15.8 ± 8.7 %

Figure 6. a) Fluorescence microscopy images of HeLa, NHDF and TGP-1 cells treated with GCPLL-*Cur-Rhod* 100 µg.mL^{-1}. Blue channel corresponds to the cell nucleus stained with DAPI, green channel corresponds to *Cur*, red channel corresponds to GCPLL MLWVs stained with *Rhod.* b) Flow cytometry FACS data of HeLa, NHDF and THP-1 cells incubated with 100 µg.mL^{-1} GCPLL-*Rhod* and GCPLL-*Cur-Rhod* MLWVs. Quantitative results show mean ± SD values of triplicates for each cell line tested.

2.5. GCPLL MLWVs can efficiently deliver chemotherapeutic compounds

The encouraging results showing the cytotoxicity of curcumin-loaded GCPLL MLWV against HeLa cells motivated further work in exploring the possibility to employ this system for drug delivery. We then assessed the encapsulation feasibility and toxicity of GCPLL MLWVs using a wider variety of chemotherapeutic compounds with different degrees of hydrophobicity. For instance, we tested these properties using standard anticancer drugs, namely doxorubicin (DOX, logP= 1.41) [58], paclitaxel (PAC, logP= 3) [59], and docetaxel (DOC, logP= 2.4) [60] on HeLa and NHDF cells. Using GCPLL-DOX MLWVs at 122 µg.mL^{-1}, there was a decrease in HeLa cell viability, accounting for only 26.8 ± 1.7 % viable cells, when compared to empty GCPLL MLWVs, with 89.5 ± 3 % viable cells (Table 2). Regarding NHDF, cell viability decreased down to 69.3 ± 0.9 % when DOX loaded vesicles was used. In comparison, unloaded vesicles did not impact cell viability. For GCPLL-PAC and GCPLL-DOC treatments at 122 µg.mL^{-1}, both loaded systems showed a cell viability higher than 65 % for NHDF. However, when HeLa cells were treated, the cytotoxic effect was observed with a cell viability measured at 59.3 ± 0.6 % and 44.3 ± 1.3 %, respectively. Both PAC and DOC loaded systems exhibited a lower cytotoxicity compared with that obtained with DOX.

Table 2. Cell viability data from Doxorubicin (DOX), Paclitaxel (PAC) and Docetaxel (DOC) delivery experiments tested on HeLa cells and NHDF cells, treated with prepared concentrations of 100 µg/mL (50 µg/mL) and 250 µg/mL (125 µg/mL) of GCPLL MLWVs. Results expressed as mean ± SEM (n=3).

Cell viability ± SEM (%)	HeLa cells		NHDF cells	
	100 µg/mL	250 µg/mL	100 µg/mL	250 µg/mL
GCPLL	93.3 ± 6.9	89.5 ± 3.0	95.9 ± 2.9	98.7 ± 1.3
GCPLL-DOX	66.9 ± 1.8	26.8 ± 1.7	81.3 ± 1.4	69.3 ± 0.9
GCPLL-PAC	98.7 ± 1.2	59.3 ± 0.6	91.6 ± 5.6	77.7 ± 6.2
GCPLL-DOC	79.5 ± 8.1	44.3 ± 1.3	85.5 ± 4.2	67.0 ± 2.0

Conclusions

This study demonstrates that microbial glycolipid amphiphiles with the ability to assemble into membranes can be used to prepare colloidal drug carriers in the absence of a phospholipid-based scaffold. Multilamellar wall vesicle colloids (MLWVs) were prepared from a monounsaturated single-glucose lipid (GC) complexed with polylysine (PLL), a biocompatible polyelectrolyte. MLWVs are stable at physiological pH in cell culture medium. Curcumin (*Cur*), a natural lipophilic drug model, was efficiently (60 %) encapsulated in the MLWVs, which show a greater therapeutic effect compared to free *Cur* treatments. The vesicles interact more efficiently with dividing cells (Hela and NHDF) than with no dividing ones (macrophages). In addition, the cytotoxic effect of curcumin is exclusive to cancerous HeLa cells, because the viability of fibroblasts and macrophages is not affected by *Cur*-loaded MLWVs. This suggests that *Cur*-loaded systems may increase the circulation time of lipophilic drugs in the bloodstream when they are confined within the MLWVs, therefore potentially reducing unwanted cytotoxic side effects. Last, GCPLL MLWVs are able to efficiently deliver other chemotherapeutic drugs (Doxorubicin, Paclitaxel and Docetaxel). This work shows that microbial glycolipid amphiphiles can be used as stand-alone soft drug carriers. It is believed that in terms of perspectives, the pH responsivity of this class of molecules is a property that can be exploited in future work to develop pH-responsive glycolipid carriers.

Author Contributions

S. A. dC., C. H. and N. B. contributed to the design of the study. S. A. dC., C. S., K. O., J. D., L. R. and J. P. conducted experiments and data analysis. S. A. dC., J. D., L. R., J. P., C. H. and N. B. provided technical advice and interpretation of results. S. A. dC., C. H., N. B. and S. O. F. wrote the manuscript and Supporting Information. All the authors commented on and amended both documents. All the authors discussed and contributed to the work.

Conflicts of interest

There are no conflicts of interest to declare.

Acknowledgements

This work was supported by French state funds managed by the Agence Nationale de la Recherche (ANR) within the Investissements d'Avenir program under reference ANR-11-IDEX-0004-02 and more specifically within the framework of the Cluster of Excellence MATISSE. ANR also supported this project within the framework of SELFAMPHI 19-CE43-0012-01.

References

1. Desai JD, Banat IM. Microbial production of surfactants and their commercial potential. *Microbiol Mol Biol Rev*. 1997;61(1):47-64. doi:10.1128/mmbr.61.1.47-64.1997

2. Rodrigues- LR, Rodrigues LR, Teixeira JA. Biomedical and Therapeutic Applications of A Biosurfactants. *Adv Exp Med Biol*. 2010;672:75-87.
3. Haque F, Khan MSA, AlQurashi N. ROS-Mediated Necrosis by Glycolipid Biosurfactants on Lung, Breast, and Skin Melanoma Cells. *Front Oncol*. 2021;11:1-13. doi:10.3389/fonc.2021.622470
4. Thakur P, Saini NK, Thakur VK, Gupta VK, Saini R V., Saini AK. Rhamnolipid the Glycolipid Biosurfactant: Emerging trends and promising strategies in the field of biotechnology and biomedicine. *Microb Cell Fact*. 2021;20(1):1-15. doi:10.1186/s12934-020-01497-9
5. Fu SL, Wallner SR, Bowne WB, et al. Sophorolipids and Their Derivatives Are Lethal Against Human Pancreatic Cancer Cells. *J Surg Res*. 2008;148(1):77-82. doi:10.1016/j.jss.2008.03.005
6. Callaghan B, Lydon H, Roelants SLKW, et al. Lactonic sophorolipids increase tumor burden in Apcmin+/- mice. *PLoS One*. 2016;11(6):e0156845. doi:10.1371/journal.pone.0156845
7. Rodrigues LR. Microbial surfactants: Fundamentals and applicability in the formulation of nano-sized drug delivery vectors. *J Colloid Interface Sci*. 2015;449:304-316. doi:10.1016/j.jcis.2015.01.022
8. Nakanishi M, Inoh Y, Kitamoto D, Furuno T. Nano vectors with a biosurfactant for gene transfection and drug delivery. *J Drug Deliv Sci Technol*. 2009;19(3):165-169. doi:10.1016/S1773-2247(09)50031-7
9. Sanches BCP, Rocha CA, Bedoya JGM, et al. Rhamnolipid-based liposomes as promising nano-carriers for enhancing the antibacterial activity of peptides derived from bacterial toxin-antitoxin systems. *Int J Nanomedicine*. 2021;16:925-939. doi:10.2147/IJN.S283400
10. Ortiz A, Teruel JA, Espuny MJ, Marqués A, Manresa Á, Aranda FJ. Interactions of a bacterial biosurfactant trehalose lipid with phosphatidylserine membranes. *Chem Phys Lipids*. 2009;158(1):46-53. doi:10.1016/j.chemphyslip.2008.11.001
11. Ortiz A, Teruel JA, Manresa Á, Espuny MJ, Marqués A, Aranda FJ. Effects of a bacterial trehalose lipid on phosphatidylglycerol membranes. *Biochim Biophys Acta - Biomembr*. 2011;1808(8):2067-2072. doi:10.1016/j.bbamem.2011.05.003
12. Otzen DE. Biosurfactants and surfactants interacting with membranes and proteins: Same but different? *Biochim Biophys Acta - Biomembr*. 2017;1859(4):639-649. doi:10.1016/j.bbamem.2016.09.024
13. Müller F, Hönzke S, Luthardt WO, et al. Rhamnolipids form drug-loaded nanoparticles for dermal drug delivery. *Eur J Pharm Biopharm*. 2017;116:31-37. doi:10.1016/j.ejpb.2016.12.013
14. Baccile N, Selmane M, Le Griel P, et al. PH-Driven Self-Assembly of Acidic Microbial Glycolipids. *Langmuir*. 2016;32(25):6343-6359. doi:10.1021/acs.langmuir.6b00488
15. Baccile N, Seyrig C, Poirier A, Alonso-De Castro S, Roelants SLKW, Abel S. Self-assembly, interfacial properties, interactions with macromolecules and molecular modelling and simulation of microbial bio-based amphiphiles (biosurfactants). A tutorial review. *Green Chem*. 2021;23(11):3842-3944. doi:10.1039/d1gc00097g
16. Safinya CR. Structures of lipid-DNA complexes: Supramolecular assembly and gene delivery. *Curr Opin Struct Biol*. 2001;11(4):440-448. doi:10.1016/S0959-440X(00)00230-X
17. Baccile N, Poirier A, Seyrig C, et al. Chameleonic amphiphile: The unique multiple self-assembly properties of a natural glycolipid in excess of water. *J Colloid Interface Sci*. 2023;630:404-415. doi:10.1016/j.jcis.2022.07.130
18. Seyrig C, Kignelman G, Thielemans W, et al. Stimuli-Induced Nonequilibrium Phase Transitions in Polyelectrolyte-Surfactant Complex Coacervates. *Langmuir*. 2020;36(30):8839-8857. doi:10.1021/acs.langmuir.0c01177
19. Seyrig C, Le Griel P, Cowieson N, Perez J, Baccile N. Synthesis of multilamellar walls vesicles polyelectrolyte-surfactant complexes from pH-stimulated phase transition using microbial biosurfactants. *J Colloid Interface Sci*. 2020;580:493-502. doi:10.1016/j.jcis.2020.07.021
20. Majumder J, Minko T. Multifunctional and stimuli-responsive nanocarriers for targeted therapeutic delivery. *Expert Opin Drug Deliv*. 2021;18(2):205-227. doi:10.4049/jimmunol.1801473.The

21. Metkar SP, Fernandes G, Navti PD, et al. Nanoparticle drug delivery systems in hepatocellular carcinoma: A focus on targeting strategies and therapeutic applications. *OpenNano*. 2023;12:100159. doi:10.1016/j.onano.2023.100159
22. Filipczak N, Pan J, Yalamarty SSK, Torchilin VP. Recent advancements in liposome technology. *Adv Drug Deliv Rev*. 2020;156:4-22. doi:10.1016/j.addr.2020.06.022
23. Kopeček J, Yang J. Polymer nanomedicines. *Adv Drug Deliv Rev*. 2020;156:40-64. doi:10.1016/j.addr.2020.07.020
24. Patel HS, Shaikh SJ, Ray D, et al. Structural transitions in mixed Phosphatidylcholine/Pluronic micellar systems and their in vitro therapeutic evaluation for poorly water-soluble drug. *J Mol Liq*. 2022;364:120003. doi:10.1016/j.molliq.2022.120003
25. Hwang D, Ramsey JD, Kabanov A V. Polymeric micelles for the delivery of poorly soluble drugs: From nanoformulation to clinical approval. *Adv Drug Deliv Rev*. 2020;156:80-118. doi:10.1016/j.addr.2020.09.009
26. Varanko A, Saha S, Chilkoti A. Recent trends in protein and peptide-based biomaterials for advanced drug delivery. 2020;156:133-187.
27. Luther DC, Huang R, Jeon T, et al. Delivery of drugs, proteins, and nucleic acids using inorganic nanoparticles. *Adv Drug Deliv Rev*. 2020;156(2020):188-213. doi:10.1016/j.addr.2020.06.020
28. KK J. An Overview of Drug Delivery Systems. In: *Methods in Molecular Biology 2059: Drug Delivery Systems*. ; 2011:1-54. doi:10.1201/b10846
29. Jamalpoor Z, Ahmadi H, Heydari M, Abdouss M, Rahdar A, Díez-Pascual AM. Chitosan based niosomal hydrogel with polyethylene glycol and halloysite nanotubes for curcumin delivery. *J Mol Liq*. 2024;401(November 2023):124640. doi:10.1016/j.molliq.2024.124640
30. Sercombe L, Veerati T, Moheimani F, Wu SY, Sood AK, Hua S. Advances and challenges of liposome assisted drug delivery. *Front Pharmacol*. 2015;6(286):1-13. doi:10.3389/fphar.2015.00286
31. Senapati S, Mahanta AK, Kumar S, Maiti P. Controlled drug delivery vehicles for cancer treatment and their performance. *Signal Transduct Target Ther*. 2018;3(1):1-19. doi:10.1038/s41392-017-0004-3
32. Li Q, Li X, Zhao C. Strategies to Obtain Encapsulation and Controlled Release of Small Hydrophilic Molecules. *Front Bioeng Biotechnol*. 2020;8:1-6. doi:10.3389/fbioe.2020.00437
33. Pourmadadi M, Abbasi P, Eshaghi MM, et al. Curcumin delivery and co-delivery based on nanomaterials as an effective approach for cancer therapy. *J Drug Deliv Sci Technol*. 2022;78(October):103982. doi:10.1016/j.jddst.2022.103982
34. Saerens KMJ, Zhang J, Saey L, Bogaert INA Van, Soetaert W. Cloning and functional characterization of the UDP-glucosyltransferease UgtB I involved in sophorolipid production by Candida bambicola and creation of a glucolipid-producing yeast strain. *Yeast*. 2011;28:279-292. doi:10.1002/yea
35. Novaira AI, Avila V, Montich GG, Previtali CM. Fluorescence quenching of anthracene by indole derivatives in phospholipid bilayers. *J Photochem Photobiol B Biol*. 2001;60(1):25-31. doi:10.1016/S1011-1344(01)00112-9
36. Leonard-Latour M, Morelis RM, Coulet PR. Influence of pyrene-based fluorescent probes on the characteristics of DMPA/DMPC Langmuir-Blodgett films. *Langmuir*. 1996;12(20):4797-4802. doi:10.1021/la960072x
37. Nandi U, Onyesom I, Douroumis D. An in vitro evaluation of antitumor activity of sirolimus-encapsulated liposomes in breast cancer cells. *J Pharm Pharmacol*. 2021;73(3):300-309. doi:10.1093/jpp/rgaa061
38. Wang W, Shu GF, Lu KJ, et al. Flexible liposomal gel dual-loaded with all-trans retinoic acid and betamethasone for enhanced therapeutic efficiency of psoriasis. *J Nanobiotechnology*. 2020;18(1):1-14. doi:10.1186/s12951-020-00635-0
39. Feng T, Wei Y, Lee RJ, Zhao L. Liposomal curcumin and its application in cancer Physical property. *Int J Nanomedicine*. 2017;12:6027-6044.
40. Patil S, Sandberg A, Heckert E, Self W, Seal S. Protein adsorption and cellular uptake of cerium

oxide nanoparticles as a function of zeta potential. *Biomaterials*. 2007;28(31):4600-4607. doi:10.1016/j.biomaterials.2007.07.029
41. Puttipipatkhachorn S, Nunthanid J, Yamamoto K, Peck GE. Drug physical state and drug-polymer interaction on drug release from chitosan matrix films. *J Control Release*. 2001;75(1-2):143-153. doi:10.1016/S0168-3659(01)00389-3
42. Tomeh MA, Hadianamrei R, Zhao X. A review of curcumin and its derivatives as anticancer agents. *Int J Mol Sci*. 2019;20(5). doi:10.3390/ijms20051033
43. Goel A, Kunnumakkara AB, Aggarwal BB. Curcumin as "Curecumin": From kitchen to clinic. *Biochem Pharmacol*. 2008;75(4):787-809. doi:10.1016/j.bcp.2007.08.016
44. Herger M, Van GR, M B, MC M. The Molecular Basis for the Pharmacokinetics and Pharmacodynamics of Curcumin and its Metabolites in Relation to Cancer. *Cancer Pharmacol Rev*. 2014;66(222-307).
45. Kalepu S, Nekkanti V. Insoluble drug delivery strategies: Review of recent advances and business prospects. *Acta Pharm Sin B*. 2015;5(5):442-453. doi:10.1016/j.apsb.2015.07.003
46. Quitschke WW. Differential solubility of curcuminoids in serum and albumin solutions: Implications for analytical and therapeutic applications. *BMC Biotechnol*. 2008;8:1-17. doi:10.1186/1472-6750-8-84
47. Barry J, Fritz M, Brender JR, Smith PES, Lee DK, Ramamoorthy A. Determining the effects of lipophilic drugs on membrane structure by solid-state NMR spectroscopy: The case of the antioxidant curcumin. *J Am Chem Soc*. 2009;131(12):4490-4498. doi:10.1021/ja809217u
48. Tsukamoto M, Kuroda K, Ramamoorthy A, Yasuhara K. Modulation of raft domains in a lipid bilayer by boundary-active curcumin. *Chem Commun*. 2014;50(26):3427-3430. doi:10.4049/jimmunol.1801473.The
49. Karthikeyan A, Senthil N, Min T. Nanocurcumin: A Promising Candidate for Therapeutic Applications. *Front Pharmacol*. 2020;11:1-24. doi:10.3389/fphar.2020.00487
50. Ben Messaoud G, Le Griel P, Prévost S, et al. Single-molecule lamellar hydrogels from bolaform microbial glucolipids. *Soft Matter*. 2020;16(10):2528-2539. doi:10.1039/c9sm02158b
51. Nicholas AR, Scott MJ, Kennedy NI, Jones MN. Effect of grafted polyethylene glycol (PEG) on the size, encapsulation efficiency and permeability of vesicles. *Biochim Biophys Acta - Biomembr*. 2000;1463(1):167-178. doi:10.1016/S0005-2736(99)00192-3
52. Kulkarni S, Betageri G V., Singh M. Factors affecting microencapsulation of drugs in liposomes. *J Microencapsul*. 1995;12:229-246.
53. Sun B, Chiu DT. Determination of the encapsulation efficiency of individual vesicles using single-vesicle photolysis and confocal single-molecule detection. *Anal Chem*. 2005;77(9):2770-2776. doi:10.1021/ac048439n
54. Huang Q, Zhang L, Sun X, Zeng K, Li J, Liu YN. Coating of carboxymethyl dextran on liposomal curcumin to improve the anticancer activity. *RSC Adv*. 2014;4(103):59211-59217. doi:10.1039/c4ra11181h
55. Saengkrit N, Saesoo S, Srinuanchai W, Phunpee S, Ruktanonchai UR. Influence of curcumin-loaded cationic liposome on anticancer activity for cervical cancer therapy. *Colloids Surfaces B Biointerfaces*. 2014;114:349-356. doi:10.1016/j.colsurfb.2013.10.005
56. Foroozandeh P, Aziz AA. Insight into Cellular Uptake and Intracellular Trafficking of Nanoparticles. *Nanoscale Res Lett*. 2018;13(339). doi:10.1186/s11671-018-2728-6
57. Manzanares D, Ceña V. Endocytosis: The nanoparticle and submicron nanocompounds gateway into the cell. *Pharmaceutics*. 2020;12(4):1-22. doi:10.3390/pharmaceutics12040371
58. Doxorubicin hydrochloride. DrugBank Online. (Accessed: 31st January 2024). Available at: https://go.drugbank.com/salts/DBSALT000060.
59. Paclitaxel: Uses, Interactions, Mechanisms of Action. DrugBank Online. (Accessed: 31st January 2024). Available at: https://go.drugbank.com/drugs/DB01229.
60. Docetaxel: Uses, Interactions, Mechanisms of Action. DrugBank Online. (Accessed: 31st January 2024). Available at: https://go.drugbank.com/drugs/DB01248.

Supporting Information

Multilamellar Nanovectors composed of Microbial Glycolipid-Polylisine Complexes for Drug Encapsulation

Silvia Alonso-de-Castro[a], Sergio Oliveira Formoso[a], Chloé Seyrig[a], Korin Ozkaya[a], Julien Dumont[b], Luisa Riancho[c], Javier Perez[d], Christophe Hélary[a,*], Niki Baccile[a,*]

[a] Sorbonne Université, Centre National de la Recherche Scientifique, Laboratoire de Chimie de la Matière Condensée de Paris, LCMCP, F-75005 Paris, France

[b] Centre interdisciplinaire de recherche biologique, Collège de France, 75005 Paris, France

[c] Centre de Recherche INSTITUT DE LA VISION, UMR_S968 Inserm / UPMC / CHNO des Quinze-Vingts, 75012, Paris, France

[d] Synchrotron Soleil, L'Orme des Merisiers, Saint-Aubin, BP48, 91192 Gif-sur-Yvette Cedex, France

^{1}H NMR

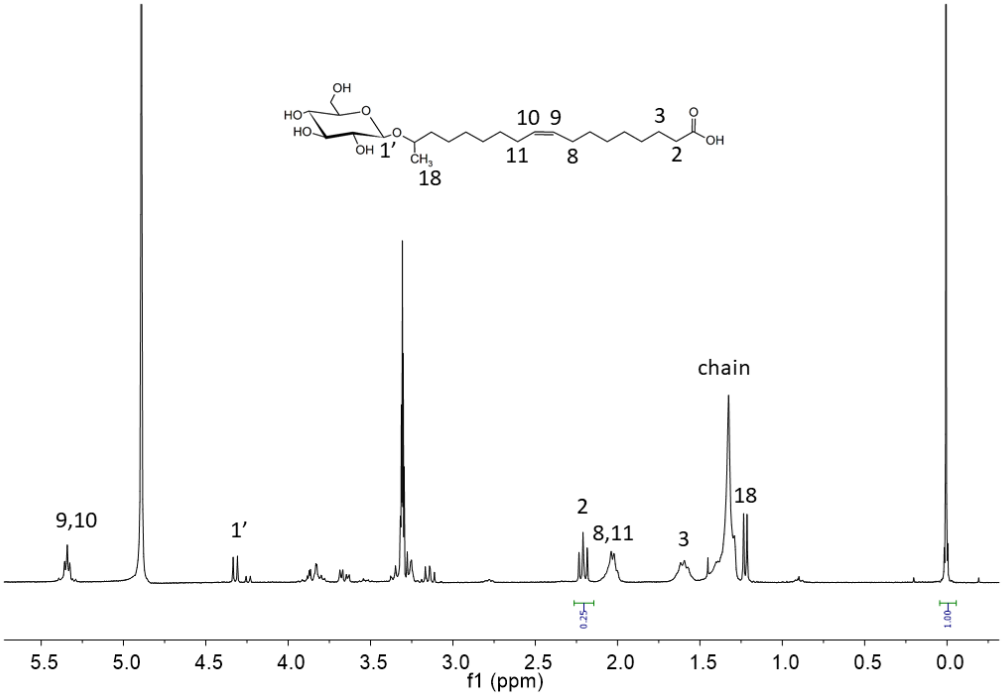

Figure S1. ^{1}H NMR of control GC in methanol-*d*$_4$.

.

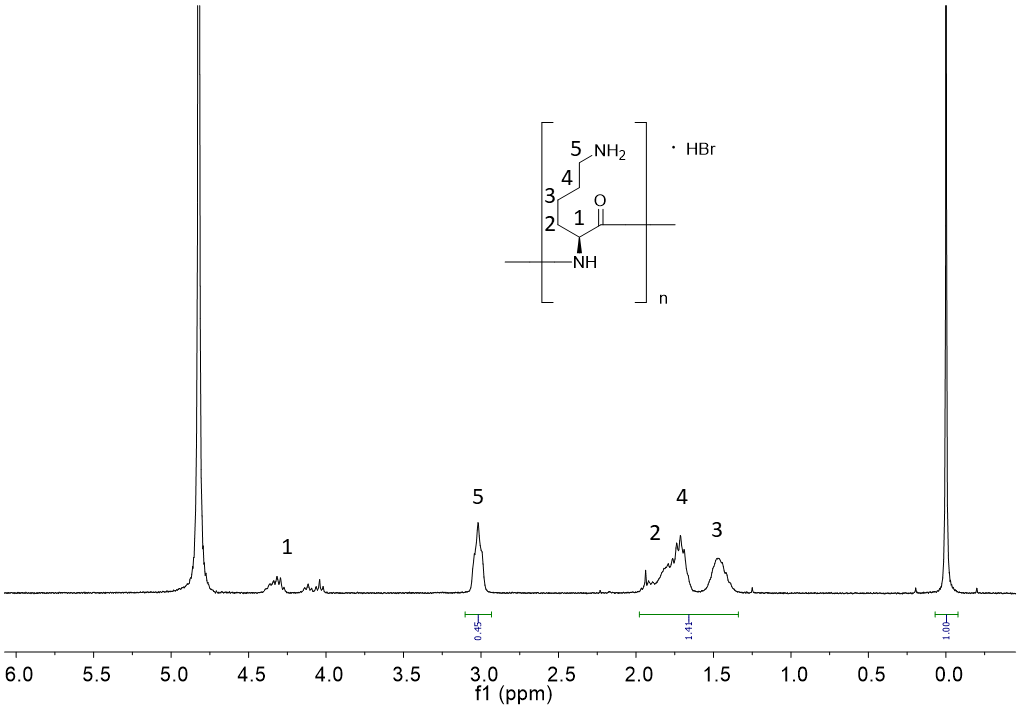

Figure S2. ^{1}H NMR of control PLL in D$_2$O.

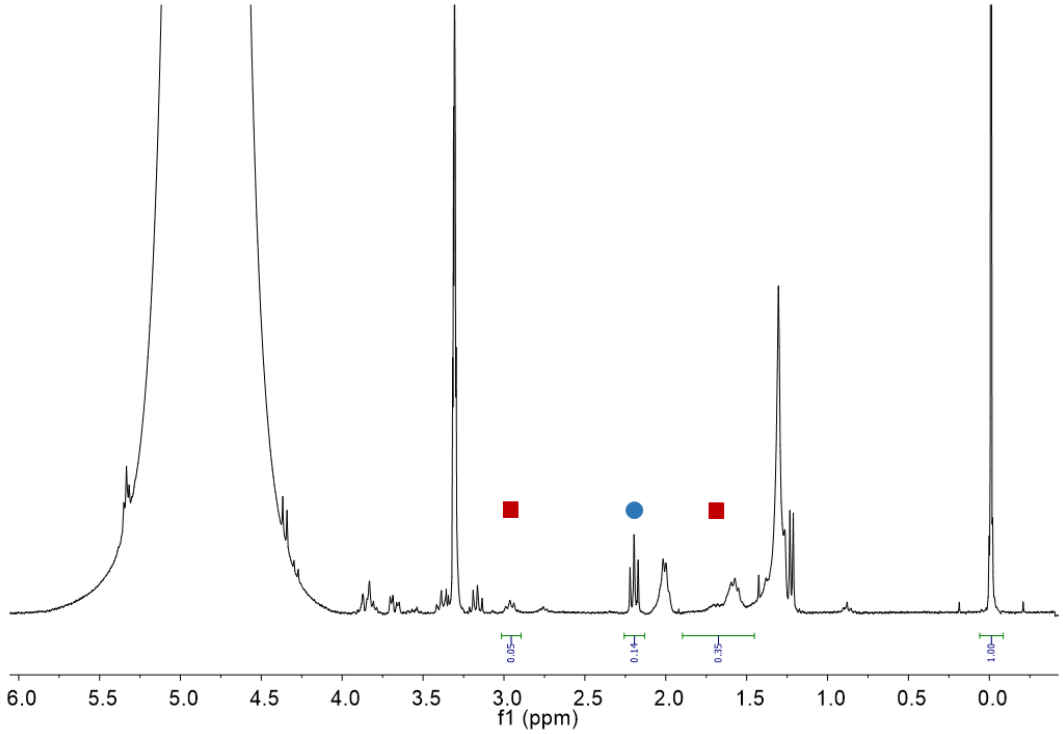

Figure S3. ^{1}H NMR from sample GCPLL in H_2O, centrifuged pellet and dissolved in methanol-d_4, where peaks assigned with ■ and ● correspond to PLL and GC, respectively.

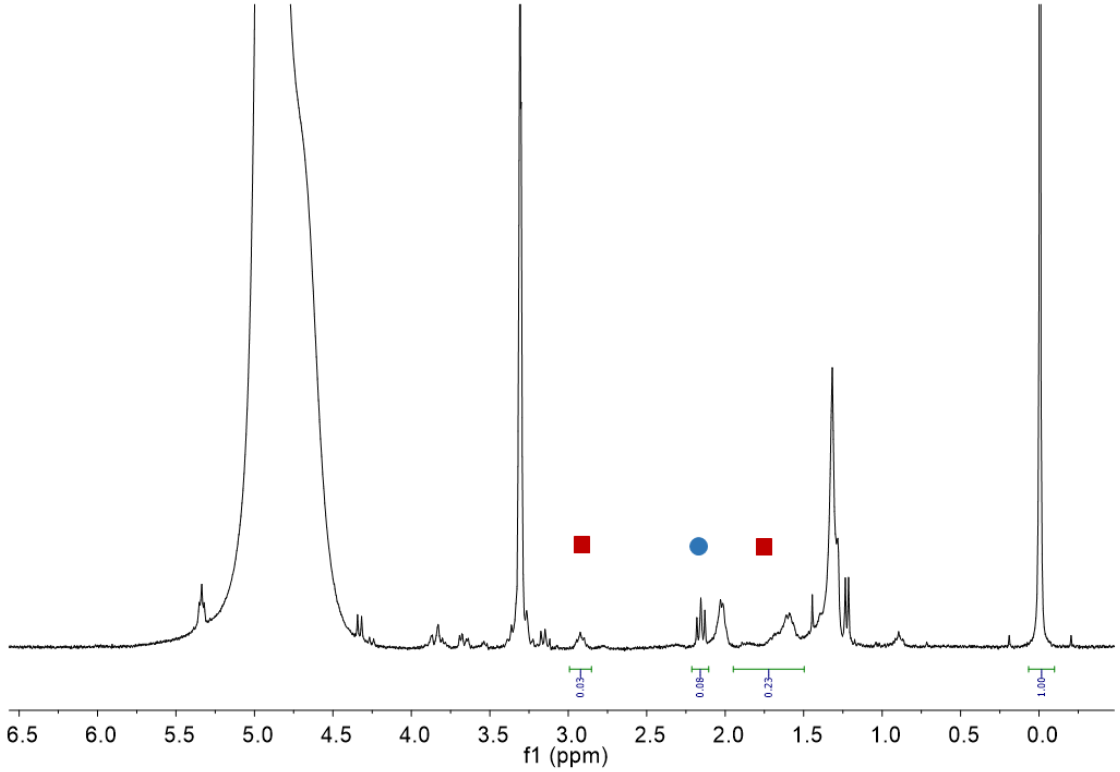

Figure S4 ^{1}H NMR from sample GCPLL in DMEM, centrifuged and dissolved in methanol-d_4, where peaks assigned with ■ and ● correspond to PLL and GC, respectively.

Table S1. Quantitative analysis of the integrals corresponding to the ^{1}H NMR spectra of the GCPLL prepared in H_2O (pH 5) and DMEM cell culture media (pH 7.5) and the resulting pellet dissolved in MeOD-d_4, shown in Figures S1-4. PLL is represented by the $(RC\underline{H_2}NH_2)_x$ (where *x* ~20) peak at δ= 2.8 ppm. The *M*w (PLL)≈ 1-5KDa, then we consider an average *M*w (PLL)= 2.5kDa, whereas the *Mw* of each monomer is 128 g/mol, yielding an average of 20 monomers per PLL chain. The valence of the $(RC\underline{H_2}NH_2)_x$ (*x*~ 20) peak is then taken as 40. G-C18:1 is represented by the $RC\underline{H_2}C{=}O$ peak at δ= 2.2ppm. The *M*w (G-C18:1)= 460 g/mol and each G-C18:1 bears a single COOH group. The valence of the $RC\underline{H_2}C{=}O$ peak is then taken as 2. The peak at δ= 0 ppm corresponds to the reference (TMSP-*d*$_4$, 1 mg.mL^{-1} ≡ 5.8mM), having a valence of 9.

	Integrals			$C_{initial}$ (mM)		C_{final} (mM)		C_F/C_{In} (%)		Molar ratio		Functional group
	GC (2H)	PLL (40H)	TMSP-d4 (9H)	$[GC]_{in}$	$[PLL]_{in}$	$[GC]_f$	$[PLL]_f$	$GC_{f/in}$	$PLL_{f/in}$	GC_{in}/PLL_{in}	GC_f/PLL_f	$[COOH]/[NH_2]$
H_2O	0.14	0.05	1	5.4	1	3.7	0.065	70	6.5	5.4	57	2.8
DMEM	0.09	0.03	1	5.4	1	2.4	0.04	45	4	5.4	60	3

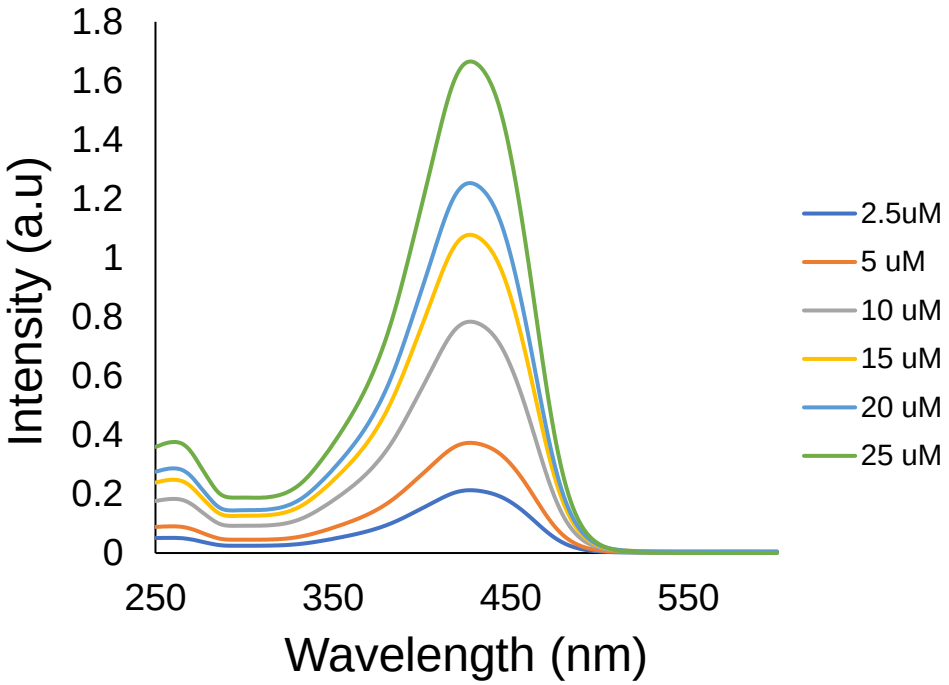

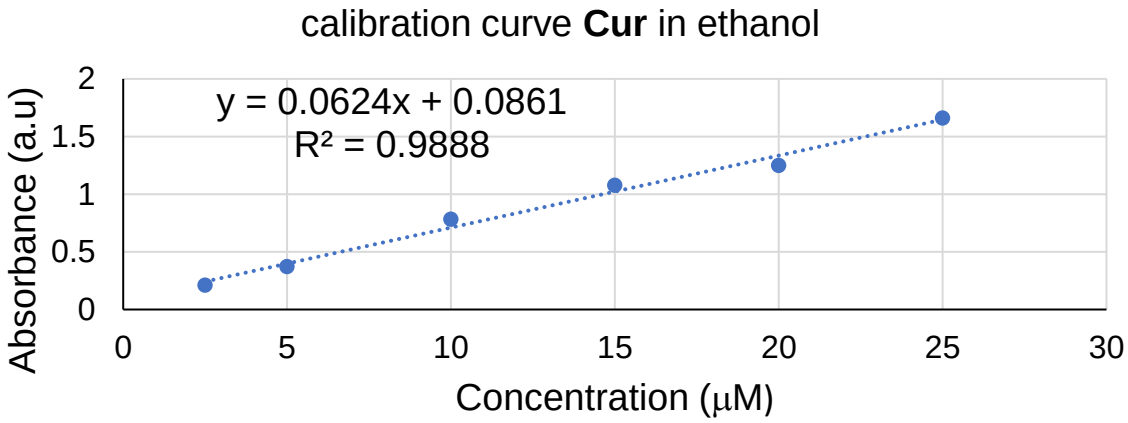

Figure S5. UV-Vis spectra of the calibration curve of *Cur* in ethanol.

Fluorescence Microscopy

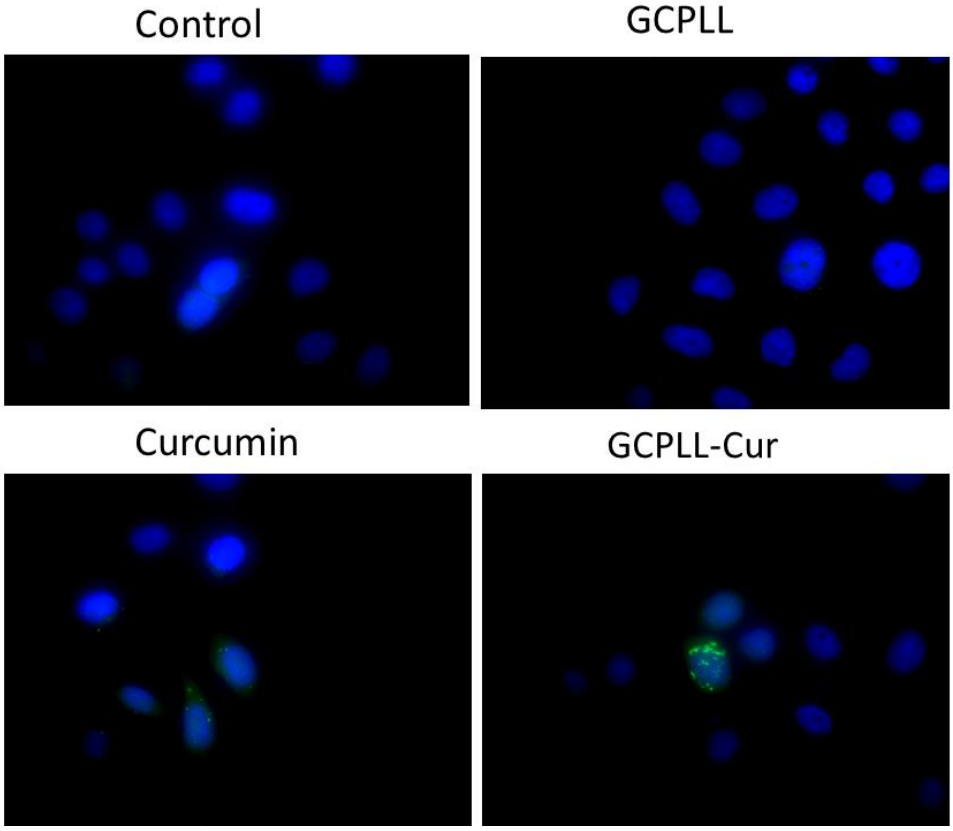

Figure S6. Fluorescence microscopy of Hela cells stained with DAPI for nucleus.

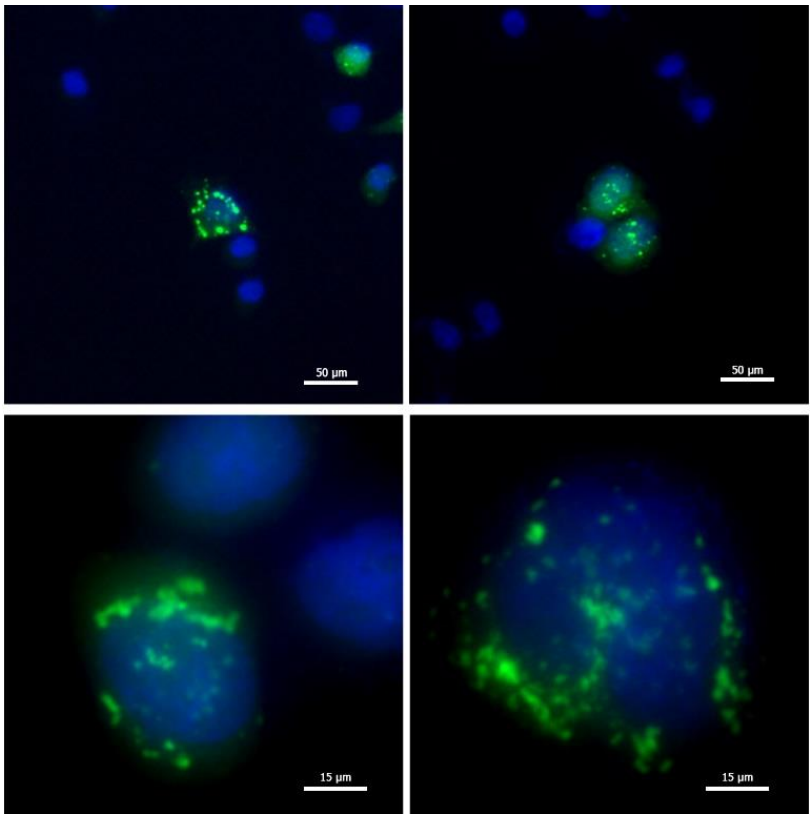

Figure S7. Fluorescence microscopy images of Hela cells stained with DAPI for nucleus after incubation with GCPLL-*Cur* MLWVs.*Cur* is in green.